Force-induced breakdown of flexible polymerized membrane

J. Paturej,[1,2] H. Popova,[3] A. Milchev,[1,3] and T. A. Vilgis[1]
[1]*Max Planck Institute for Polymer Research, 10 Ackermannweg, D-55128 Mainz, Germany*
[2]*Institute of Physics, University of Szczecin, Wielkopolska 15, PL-70451 Szczecin, Poland*
[3]*Institute of Physical Chemistry, Bulgarian Academy of Sciences, BG-1113 Sofia, Bulgaria*
(Received 28 November 2011; published 21 February 2012)

We consider the fracture of a free-standing two-dimensional (2D) elastic-brittle network to be used as protective coating subject to constant tensile stress applied on its rim. Using a molecular-dynamics simulation with a Langevin thermostat, we investigate the scission and recombination of bonds, and the formation of cracks in the 2D graphenelike hexagonal sheet for different pulling force f and temperature T. We find that bond rupture occurs almost always at the sheet periphery, and the first mean breakage time $\langle\tau\rangle$ of bonds decays with membrane size as $\langle\tau\rangle \propto N^{-\beta}$, where $\beta \approx 0.50 \pm 0.03$ and N denotes the number of atoms in the membrane. The probability distribution of bond scission times t is given by a Poisson function $W(t) \propto t^{1/3}\exp(-t/\langle\tau\rangle)$. The mean failure time $\langle\tau_r\rangle$ necessary to rip off the sheet declines with growing size N as a power law $\langle\tau_r\rangle \propto N^{-\phi(f)}$. We also find $\langle\tau_r\rangle \propto \exp(\Delta U_0/k_BT)$, where the nucleation barrier for crack formation $\Delta U_0 \propto f^{-2}$, in agreement with Griffith's theory. $\langle\tau_r\rangle$ displays an Arrhenian dependence of $\langle\tau_r\rangle$ on temperature T. Our results indicate a rapid increase in crack spreading velocity with growing external tension f.

DOI: 10.1103/PhysRevE.85.021805 PACS number(s): 82.35.Lr

I. INTRODUCTION

Fracture in engineering materials is a long-standing topic of research due to problems that arise with technological applications and the ensuing economic implications. Thus, for decades a lot of attention has been focused on understanding the macroscopic and microscopic factors that trigger failure. Recently, interest in gaining a better understanding of the interplay between elastic and fracture properties of brittle materials has been revived due to the rapidly developing design of advanced structural materials.

Promising aspects for applications include reversible polymer networks [1,2] and also graphene, which shows unusual thermomechanical properties [3,4]. Among other things, graphene, which is a honeycomb lattice packed with C atoms, can be used as anticorrosion gas barrier protective coating [5], in chemical and biosensors [6], or as an efficient membrane for gas separation [7]. In all possible applications, the temperature and stress-dependent fracture strength of this two-dimensional (2D) network is of crucial importance. Graphene has been investigated recently by Barnard and Snook [8] using *ab initio* quantum-mechanical techniques whereby it was noted that that the problems "ha(ve) been overlooked by most computational and theoretical studies."

An important example of biological microstructure is *spectrin*, the red blood cell membrane skeleton, which reinforces the cytoplasmic face of the membrane. In erytrhrocytes, the membrane skeleton enables it to undergo large extensional deformations while maintaining the structural integrity of the membrane. A number of studies based on continuum [9], percolation [10–12], or molecular level [13–15] considerations of the mechanical breakdown of this network, modeled as a triangular lattice of spectrin tetramers, have been reported so far. Many of these studies can be viewed in a broader context as part of the problem of thermal decomposition of gels [16], epoxy resins [17,18] and other 3D networks both experimentally [16–18] and by means of simulations [19] in the case of poly-dimethylsiloxane (PDMS).

The aforementioned examples illustrate well the need for a deeper understanding of the processes of failure in brittle materials. In addition to analytical and laboratory investigations, computer simulations [20–22] have provided a lot of insight into aspects that are difficult to perceive through direct observations or theoretical treatment; for a review of previous works, see Alava *et al.* [23]. Most of these studies focus on the propagation of (preexisting) cracks, relating observations to the well-known Griffith's model [24] of crack formation. A number of important aspects of material failure have therefore received little attention. Thus only a few simulations examine the rate of crack nucleation, which involves long time scales necessary for thermal activation; see, however, [25–28]. The effects of system size on the characteristic time for bond rupture have not been examined except in a recent molecular dynamics (MD) study by Dias *et al.* [29]. Also, the recombination of broken bonds has not been considered. These and other insufficiently explored properties related to fracture have motivated our present investigation of a free-standing 2D honeycomb brittle membrane by means of MD simulation. In view of the possible applications as anticorrosion and gas barrier coating, we consider a radially spanned sheet of a regular hexagonal flake shape so as to minimize the effects of corners and unequal edge lengths that are typical for ribbonlike sheets. Tensile constant force is applied on the rim of the flake, perpendicular to each edge. By varying the system size, tensile force, and temperature, we collect a number of results that characterize the initiation and the course of fragmentation in stretched 2D honeycomb networks.

The paper is organized as follows. After a brief introduction, we sketch our model in Sec. II, where we consider interactions between atoms in the brittle honeycomb membrane, define the threshold for bond scission, and also introduce some basic quantities that are measured over the course of the simulation. In Sec. III, we present our simulation results. In Sec. III A, we present briefly the results on the recombination of broken bonds. In Sec. III B, we present the distribution of bond

scission rates over the membrane surface, the dependence of the mean first breakage time (MFBT) before a bond scission takes place and of the mean failure time until the 2D sheet breaks apart on applied tensile force, and we examine how these times depend on membrane size and temperature. The formation of cracks at different cases of applied stress as well as their propagation in a 2D honeycomb brittle sheet are briefly considered in Sec. III C. We end the paper with a brief summary of results in Sec. IV.

II. MODEL AND SIMULATION PROCEDURE

A. The model

We study a coarse-grained model of a honeycomb membrane embedded in three-dimensional (3D) space. The membrane consists of N spherical particles (beads and monomers) of diameter σ connected in a honeycomb lattice structure whereby each monomer is bonded with three nearest neighbors except for the monomers on the membrane edges, which have only two bonds [see Fig. 1 (left panel)]. The total number of monomers N in such a membrane is $N = 6L^2$, where L denotes the number of monomers (or hexagon cells) on the edge of the membrane (i.e., L characterizes the linear size of the membrane). There are altogether $N_{\text{bonds}} = (3N - 6L)/2$ bonds in the membrane. In our studies, we consider *symmetric* hexagonal membranes (i.e., *flakes*) so as to minimize possible effects due to the asymmetry of edges or vortices at the membrane periphery.

For the analysis of our results, we find it appropriate to divide the two-dimensional membrane network so that all bonds fall into different subgroups presented by concentric "circles" with consecutive numbers [see Fig. 1 (right panel)] proportional to their radial distance from the membrane center. *Odd* circle numbers thus contain bonds that are nearly tangential to the corresponding circle. *Even* circles contain no radially oriented bonds (shown to cross the circle in Fig. 1). The total number of circles C in a membrane of linear size L is found to be $C = (2L - 1)$. We use this scheme of labeling the groups of bonds that compose the membrane in order to represent our simulation results in an appropriate way that relates them to their relative proximity to the membrane's periphery.

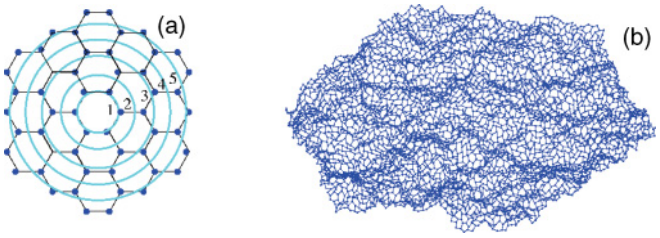

FIG. 1. (Color online) (a) A membrane with a honeycomb structure that contains a total of $N = 54$ beads and has a linear size $L = 3$ (L is the number of hexagonal cells on the edge of the membrane). (b) A snapshot of a typical conformation of an intact membrane with $L = 30$ containing 5400 monomers after equilibration with no external force applied. Typical wrinkles are seen to form on the surface.

B. Potentials

The nearest neighbors in the membrane are connected to each other by breakable anharmonic bonds described by a Morse potential,

$$U_{\text{Morse}}(r) = \epsilon_M\{1 - \exp[-\alpha(r - r_{\text{min}})]\}^2, \tag{1}$$

where r is the distance between the monomers. Here $\alpha = 1$ is a constant that determines the width of the potential well (i.e., bond elasticity) and $r_{\text{min}} = 1$ is the equilibrium bond length. The dissociation energy of a given bond, $\epsilon_M = 1$, is measured in units of k_BT, where k_B denotes the Boltzmann constant and T is the temperature. The minimum of this potential occurs at $r = r_{\text{min}}$, $U_{\text{Morse}}(r_{\text{min}}) = 0$. The maximal restoring force of the Morse potential, $f_{\text{max}} = -dU_{\text{Morse}}/dr = \alpha\epsilon_M/2$, is reached at the inflection point, $r = r_{\text{min}} + \alpha^{-1}\ln(2) \approx 2.69$. This force, f_{max}, determines the maximal tensile strength of the membranes bonds. Since $U_{\text{Morse}}(0) \approx 2.95$, the Morse potential, Eq. (1), is only weakly repulsive and beads could partially penetrate one another at $r < r_{\text{min}}$. Therefore, in order to allow properly for the excluded volume interactions between bonded monomers, we take the bond potential as a sum of $U_{\text{Morse}}(r)$ and the so called Weeks-Chandler-Anderson (WCA) potential, $U_{\text{WCA}}(r)$ (i.e., the shifted and truncated repulsive branch of the Lennard-Jones potential),

$$U_{\text{WCA}}(r) = \begin{cases} 4\epsilon\left[\left(\frac{\sigma}{r}\right)^{12} - \left(\frac{\sigma}{r}\right)^{6}\right] + \epsilon & \text{for } r \leqslant 2^{1/6}\sigma, \\ 0 & \text{for } r > 2^{1/6}\sigma, \end{cases} \tag{2}$$

with parameter $\epsilon = 1$ and monomer diameter $\sigma = 2^{-1/6} \approx 0.89$ so that the minimum of the WCA potential coincides with the minimum of the Morse potential. Thus, the length scale is set by the parameter $r_{\text{min}} = 2^{1/6}\sigma = 1$. The nonbonded interactions between monomers are taken into account by means of the WCA potential, Eq. (2). Thus, the nonbonded interactions in our model correspond to good solvent conditions, whereas the bonded interactions make the bonds breakable when subject to stretching. External stretching force f is applied to monomers at the membrane rim perpendicular to the respective edge; see Fig. 2(a).

Before we turn to the problem of membrane failure under constant tensile force, we show here some typical elastic properties of the intact honeycomb network sheet that is used in our computer experiments; see Fig. 2. In Fig. 2(b), one can see an S-shaped variation of the stress-strain relationship with initial significant elongation at vanishing stress due to the straightening of the membrane wrinkles (ripples) that are typical for an unperturbed membrane; cf. Fig. 1(b). This behavior is followed by a linear stress-strain elastic relationship where we measure the Young modulus $Y_r = 2.02 \times 10^{-2}$ (k_BT/a^3) [or $Y_u = 2.95 \times 10^{-2}$ (k_BT/a^3)], depending on whether radial of uniaxial loading is applied. Eventually, for stronger stretching, the elasticity of the network decreases as the anharmonicity of the bond potential comes into play. Moreover, Fig. 2(b) indicates that the destructive strain of the whole membrane is considerably weaker in the case of uniaxial stretching.

In our work, we have tried to develop a generic model for all kinds of 2D brittle-elastic networks with honeycomb orientation. We have been anxious to emphasize the common features of failure in materials with similar architecture but largely varying elasticity properties, e.g., from 1000 GPa graphene's

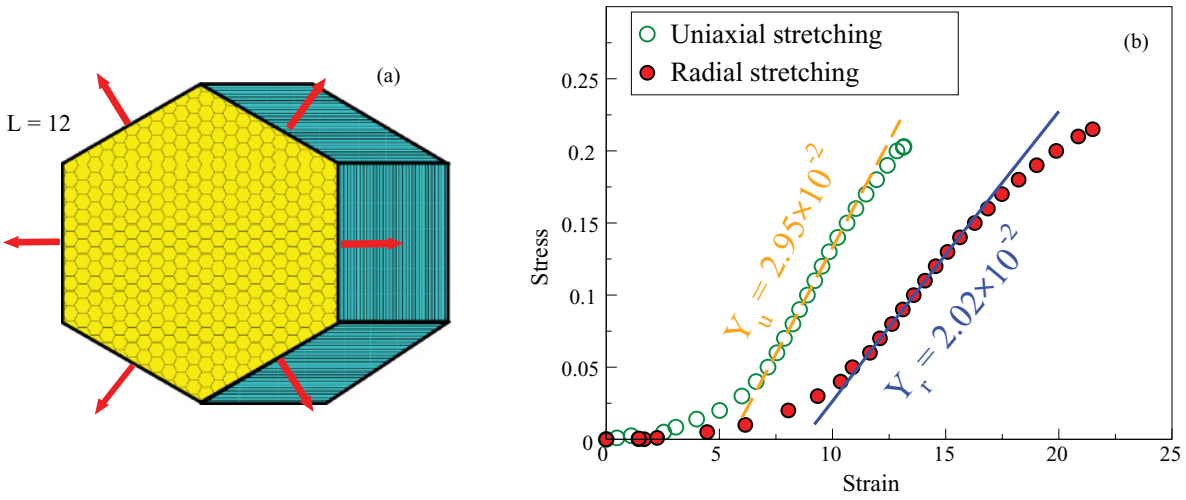

FIG. 2. (Color online) (a) A protective honeycomb network is spanned at the orifice of a prism whose size may vary due to thermal expansion. Tensile forces acting on the membrane periphery are indicated by arrows. (b) Mean strain of a honeycomb membrane of size $L = 10$ as a function of external tensile stress f at $T = 0.01$ and $\gamma = 0.25$. Depending on the way in which external force is applied—(i) radial stretching [Fig. 9(f)] or (ii) uniaxial stretching [Fig. 9(b)]—the observed Young modulus is $Y_r = 2.02 \times 10^{-2}$ (k_BT/a^3) or $Y_u = 2.95 \times 10^{-2}$ (k_BT/a^3).

Young modulus [4] compared to 4×10^{-3} GPa for spectrin [15]. Applying the value of a Kuhn segment ($\sigma = 1.44$ Å) and taking the thermal energy $k_BT = 4 \times 10^{-21}$ J at $T = 300$ K, we get from our simulation a Young modulus ~0.03 GPa, which ranges between typical values for rubberlike materials 0.01–0.1. Compared to *ab initio* simulations of graphene with linear size $L = 6$, which corresponds to 216 network nodes [8], our objects are about an order of magnitude larger, $L = 50$ and 2500 nodes, in units of elementary cells.

C. MD algorithm

As in our previous studies concerning scission kinetics of linear chains [30,31] and bottle brushes [32], we use a Langevin dynamics that describes the Brownian motion of a set of interacting particles whereby the action of the solvent is split into slowly evolving viscous (frictional) force and a rapidly fluctuating stochastic (random) force. The Langevin equation of motion is the following:

$$m\,\vec{v_i}(t) = \vec{F_i}(t) - m\gamma\,\vec{v_i}(t) + \vec{R_i}(t), \tag{3}$$

where m denotes the mass of the particles, which is set to $m = 1$, $\vec{v_i}$ is the velocity of particle i, $\vec{F_i} = (\vec{F_M} + \vec{F_{WCA}})_i$ is the conservative force, which is a sum of all forces exerted on particle i by other particles in the system, γ is the friction coefficient, and $\vec{R_i}$ is the three-dimensional vector of random force acting on particle i. The random force $\vec{R_i}$, which represents the incessant collision of the monomers with the solvent molecules, satisfies the fluctuation-dissipation theorem $\langle R_{i\alpha}(t)R_{j\beta}(t')\rangle = 2\gamma k_BT\delta_{ij}\delta_{\alpha\beta}\delta(t-t')$, where the symbol $\langle\cdots\rangle$ denotes an equilibrium average and the greek-letter subscripts refer to the x, y, or z components. The friction coefficient γ of the Langevin thermostat is set to $\gamma = 0.25$. Our simulation was performed in the weakly damped regime of $\gamma = 0.25$, where the effects of inertia are important. This value of γ is more or less standard in Langevin MD. However, we carried out additional simulation in the strongly damped regime for $\gamma = 10$. No qualitative changes were discovered except an absolute overall increase of the rupture times τ, which is natural for a more viscous environment. The integration step is 0.002 time units (t.u.) and the time is measured in units of $r_{min}\sqrt{m/\epsilon_M}$. We emphasize at this point that in our coarse-grained modeling, the solvent is taken into account only implicitly. In this work, the velocity-Verlet algorithm is used to integrate the equations of motion.

Our MD simulations are carried out in the following order. First, we prepare an equilibrated membrane conformation, starting with a fully flat configuration, Fig. 1, where each bead in the network is separated by a distance $r_{min} = 1$ equal to the equilibrium separation of the bond potential $(U_M + U_{WCA})$ [see Eqs. (1) and (2)]. The external constant force is switched on from the very beginning of the simulation. Then we start the simulation with this prepared conformation and let the membrane equilibrate with the applied force in the heat bath for a sufficiently long time (≈10^7 t.u.) at a temperature that is low enough so that the energy barrier for scission is high and the membrane stays intact. This equilibration is done in order to prepare different starting conformations for each simulation run. Once the equilibration is finished, the temperature is raised to the working one and we let the membrane equilibrate at this temperature for roughly ~20 t.u. We have checked that this time interval is sufficient for equipartition and uniform distribution of temperature to be established throughout the membrane sheet. Then the time is set to zero and we continue the simulation with this well-equilibrated membrane conformation, checking for scission of the bonds.

We measure the elapsed time τ until the first bond rupture occurs and repeat the above procedure for a large number of runs (10^3–10^4), starting each time with a new equilibrated conformation so as to sample the stochastic nature of rupture and determine the mean $\langle\tau\rangle$, which we refer to as the mean first breakage time. In the course of simulation, we also calculate properties such as the probability distribution of breaking bonds, examining their position in the membrane (a rupture probability histogram), the probability distribution function of the first breakage time $W(\tau)$ (i.e., the MFBT probability

distribution), the strain (extension) of the bonds with respect to the consecutive circle number in the membrane, as well as other quantities of interest.

In separate runs, each simulation is terminated as soon as the honeycomb sheet disintegrates into two separate parts, whereby the time it takes to "rip off" the sheet is termed "mean failure time" $\langle \tau_r \rangle$ and measured. In order to monitor the propagation of cracks, we perform also individual runs labeling breaking bonds in succession and reconstructing the crack trajectory, which is a laborious and rather involved problem.

D. Rupture criterion

An important aspect of our simulation is the recombination (self-healing) of broken bonds. The constant stretching force acting on the monomers at the membrane edges creates a well-defined activation barrier for bond scission. Direct analysis of the one-bond potential with external force, $U_{\mathrm{Morse}}(r) - fr$, indicates that the positions of the (metastable) minimum r_- and of the barrier (or hump) r_+ are given by Ref. [33]

$$r_{-,+} = \frac{1}{a} \ln\left[\frac{2}{1 \pm \sqrt{1-\tilde{f}}}\right], \tag{4}$$

where the dimensionless force $\tilde{f} = 2f/a\epsilon_M$. For the range of tensile forces used in the present study, one has typically $r_+ \approx 3r_{\min}$. The activation energy (barrier height) for single bond scission is itself given by Ref. [33]

$$\begin{aligned} E_b &= U(r_+) - U(r_-) \\ &= \epsilon_M \left\{ \sqrt{1-\tilde{f}} + \frac{\tilde{f}}{2} \ln\left[\frac{1-\sqrt{1-\tilde{f}}}{1+\sqrt{1-\tilde{f}}}\right] \right\}. \end{aligned} \tag{5}$$

One can easily verify that E_b decreases with $\tilde{f}$. Since a bond may get stretched beyond the energy barrier and nonetheless shrink back again, i.e., recombine, in our numeric experiments we use a sufficiently large value for critical extension of the

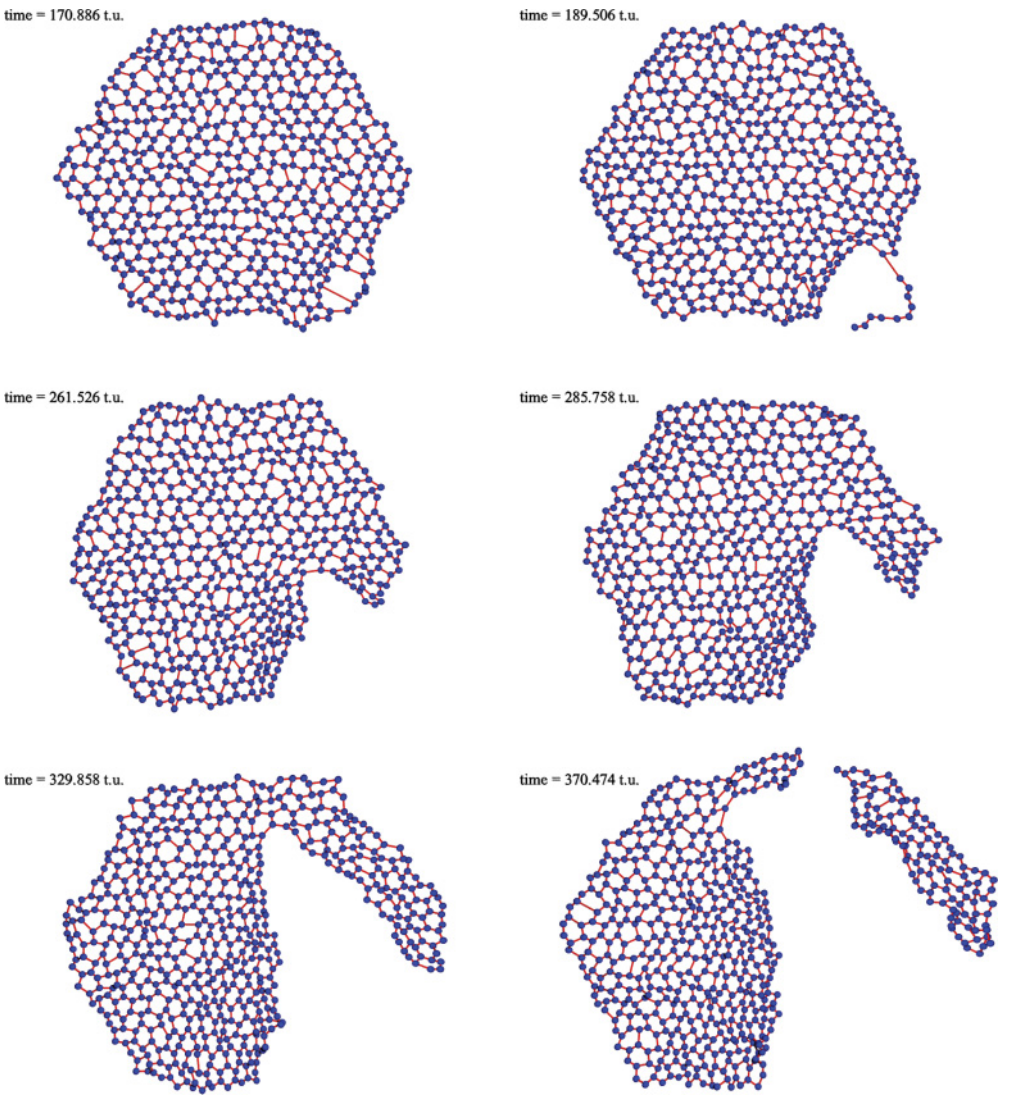

FIG. 3. (Color online) Snapshots illustrate the process of bond breakage (crack generation) in different time moments for a membrane with $N = 600$ particles subject to external tensional force $f = 0.15$ at $T = 0.05$ and $\gamma = 0.25$. The force is applied to periphery monomers only and stretches the network perpendicular to its original edges.

bonds, $r_h = 5r_{\min}$, which is defined as a threshold to a broken state of the bond. This convention is based on our checks that the probability for recombination (self-healing) of bonds, stretched beyond r_h, is vanishingly small, as demonstrated below. In our model, we deal with $E_b/(k_B T) = 20$, which at 300 K and bond length $r_{\min} = 0.14$ nm corresponds to ultimate tensile stress ~0.6 GPa. This is a reasonable value for our membrane, which is considerably softer than graphene with ~100 GPa [4] and ranges between typical values for rubber materials 0.03–14 GPa.

III. MD RESULTS

We examine the scission of bonds between neighboring nodes in the network sheet with honeycomb topology, assuming thermal activation as a driving mechanism, in agreement with early experimental work by Brenner [34] and Zhurkov [35]. In Fig. 3, we show a series of representative snapshots of a membrane of size $L = 10$ with $N = 600$ monomers taken at different time moments during the process of decomposition. Typically, the first bonds that break are observed to belong to the last (even) most remote circle as, for example, at $t \approx 171$ t.u. in Fig. 3. As mentioned above, these are the radially oriented bonds, which belong to concentric circles of even number. Gradually, a line of edge beads is then severed from the rest of the membrane and a crack is formed that propagates into the bulk until eventually a piece of the network sheet is ripped off, as in Fig. 3 at $t \approx 370$ t.u. As we shall see below, this mechanism of membrane failure, whereby an initial crack is formed parallel to the edge monomers, yet perpendicular to the tensile force, dominates largely the process of disintegration under constant tensile force. The process is, therefore, mainly described by two characteristic times, τ and τ_r, which mark the occurrence of the first scission of a bond (MFBT) and that of the eventual breakdown of the flake into two distinct parts.

A. Bond recombination

As mentioned in Sec. III, throughout our studies of the brittle sheet breakdown, we use a threshold for critical bond stretching (rupture criterion), $r_h = 5r_{\min}$. In the right inset of Fig. 4, we display the function $Q_h(h)$, which represents the probability distribution of bond stretching h beyond the hump position r_+, given that a subsequent recombination has taken place. To this end, one monitors for 10^4 integration steps the length of each bond once the bond expands beyond r_+ and stores its maximal expansion, h, provided such a bond contracts again to $r < r_+$. Then $Q_h(h)$ is computed as the fraction of extensions to h over the total number of recombination events. For each bond recombination, one measures also the distribution of the respective self-healing times, $P_h(t)$, which is shown in Fig. 4 too. Both distributions are characterized by exponentially fast decaying tails, indicating that successful recombinations are possible after a very short time interval, ≈1.3 t.u., and the possible stretching of a bond in such cases is minimal—about 0.19–0.5 beyond the energy barrier position at $r_+ \approx 2.96$, that is, significantly shorter than $r_h \approx 5$. We also find that recombination of bonds seldom takes place (roughly 1.5% over 5×10^4 runs of average length ≈437 t.u. for a membrane composed of $N = 600$ beads). Yet as indicated below, allowing for self-healing events may significantly change the observed kinetics of membrane destruction. The left inset in Fig. 4 indicates that self-healing of bonds happens most frequently at the membrane periphery, $C = 19$, where bond stretching occurs most frequently.

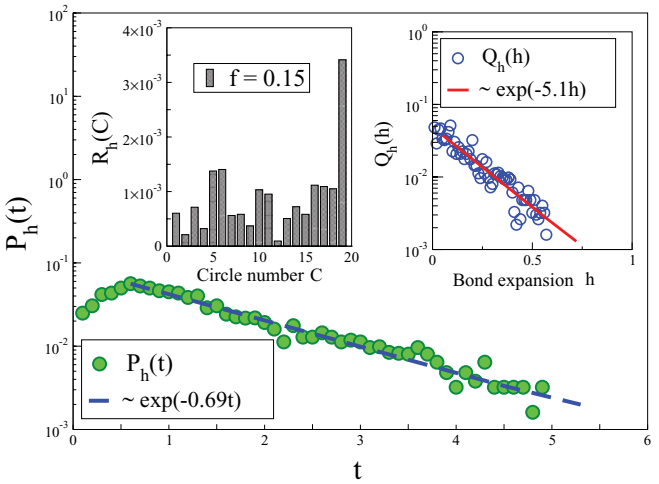

FIG. 4. (Color online) Probability distribution $P_h(t)$ of maximal times (full circles) and $Q_h(h)$ of maximal bond lengths h (empty circles, right panel of inset) before a recombination event in the stretched membrane with $N = 600$, $T = 0.1$, and $\gamma = 0.25$ takes places. The exponential tail of $P_h(t)$ is represented by a blue dashed line. The exponential decay of $Q_h(h)$ is given by a solid red line. The left panel of the inset shows the healing probability R_h vs circle number C. The healing events under applied stress occur roughly 10 times less frequently than for $f = 0$.

B. Mean first breakage time

These conclusions, based on visual evidence from snapshots taken in the course of membrane decomposition, are corroborated in Fig. 5(a), where we show the probability distribution of a first rupture for *all* bonds in the honeycomb membrane flake as a 3D plot. It is seen that the scission rate is localized in the outermost circle of radial bonds, whereas bonds in the inner part of the membrane almost never break. Note that this is not a trivial effect since tension is distributed uniformly over all bonds in the equilibrated membrane, so there is no additional propagation of the tension front from the rim toward the center. Figure 5(b) also indicates a qualitative change in the rupture PDF when self-healing is not allowed for (by reducing the threshold position to that of the energy barrier, $r_h = 3.1$), in contrast to results in which self-healing was fully taken into account, $r_h = 5$. Moreover, a closer inspection of Fig. 5(b) indicates that scission of bonds with no self-healing takes place almost uniformly throughout the membrane, while that with self-healing is concentrated only at the membrane periphery.

One can try to relate this finding to the distribution of strain within the network, as shown in Fig. 6(a) and sampled for several strengths of the external stretching force f. In the case of strongest pulling, $f = 0.15$, the variation of the mean-squared bond length $\langle l^2 \rangle$ with distance from the membrane center (i.e., with consecutive circle number C)

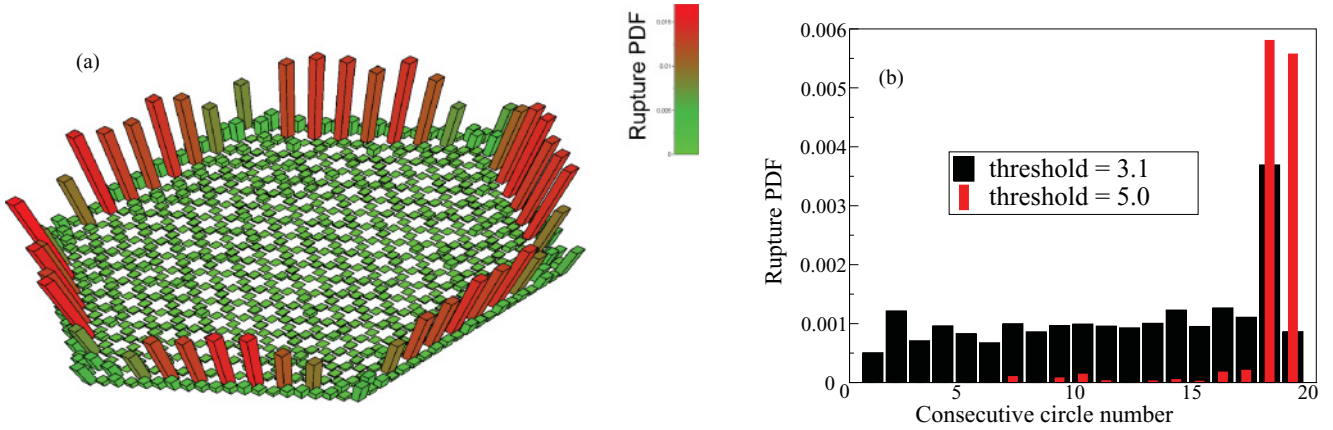

FIG. 5. (Color online) (a) Rupture probability histogram of the flexible hexagonal membrane subjected to external tensile stress $f = 0.15$. (b) Scission probability histogram vs consecutive circle number for the membrane pulled with $f = 0.125$ displayed for different rupture thresholds r_h as indicated. Real rupture events ($r_h = 5.0$) are concentrated at the periphery, whereas fictitious ones ($r_h = 3.1$) are distributed more uniformly all over the membrane. Here $N = 600$, $T = 0.05$, and $\gamma = 0.25$.

displays a well-expressed sawtooth behavior, whereby the peaks correspond to bonds with radial rather than tangential orientation (odd C). The alternation of strongly and weakly stretched bonds modulates the overall gradual increase of the mean bond length with growing distance from the center. Evidently, the amplitude of the mean-squared bond length attains a pronounced maximum on the last circle of radially oriented network bonds. This distribution of strain is found to persist down to vanishing tensile force $f = 0$; see Fig. 6(a). The distribution of first scission events is clearly seen in Fig. 6(b), where we show it for several strengths of f. Evidently, with a growing value of f, bonds also break deeper inside the membrane, although such events remain much less probable.

The variation of the MFBT τ with system size N (i.e., with the number of monomers in the membrane $N = 6L^2$, where L denotes the linear size of the flake) is shown in Fig. 7. For sufficiently large membranes, one observes a power-law decline of the MFBT, $\tau \propto N^{-\beta}$, with an exponent $\beta \approx 0.5 \pm 0.03$ for the tensile forces studied. If thermally activated bonds break independently from one another and entirely at random, then the MFBT τ measures the interval before *any* of the available intact bonds undergoes scission, that is, either the first bond breaks or the second one, and so on, which, at a constant rate of scission, would reduce the MFBT $\tau \propto 1/N$ as observed, for instance, in the case of thermal degradation of a linear polymer chain [31]. This simple result can be derived more comprehensively by means of the classical theory of Weibull. In the present system of a honeycomb membrane, the bonds that undergo rupture are nearly all located at the rim of the flake and their number is proportional to L so that with $\beta \approx 0.5$ (cf. Fig. 7) and $N \propto L^2$, one obtains eventually the important result $\tau \propto 1/L$. This observation is in agreement with recent results of Grant *et al.* [29], who studied the nucleation of cracks in a

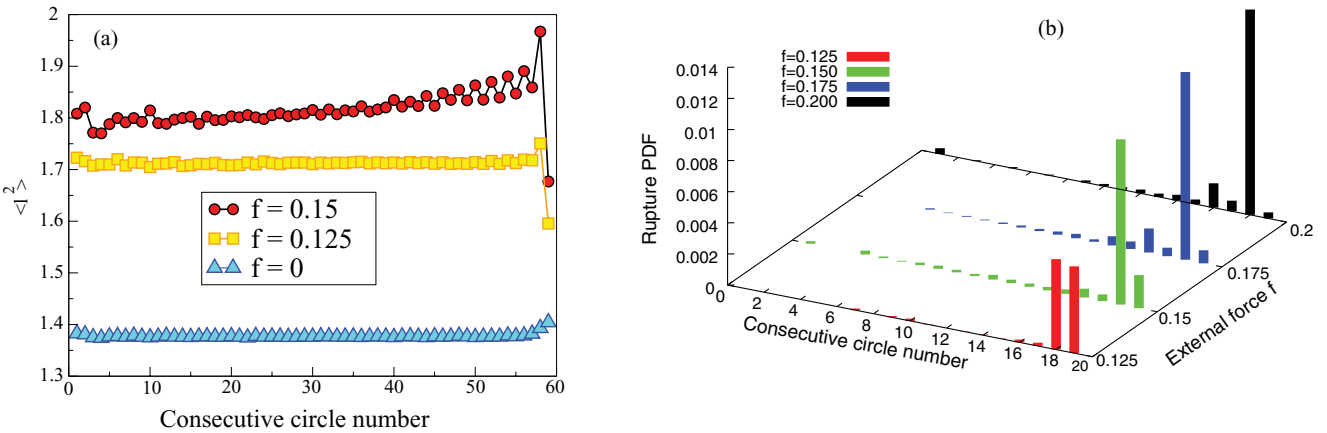

FIG. 6. (Color online) (a) Variation of the mean-squared bond length $\langle l^2 \rangle$ with consecutive circle number in a membrane with $N = 5400$ beads subjected to different strengths of the external force f (as indicated in the legend). (b) Probability distribution of the first bond scission event vs circle number in a membrane with $N = 600$ beads at different strengths of the external force f as indicated. For a force $f \leqslant 0.15$, the bonds from the last two outer circles (Nos. 18 and 19) in the membrane have the highest rupture probability. With increased strength of the pulling force $f \geqslant 0.175$, the bonds that are located in the circles Nos. 18 and 16 attain the highest rupture probability. Parameters of a heat bath are $T = 0.05$ and $\gamma = 0.25$.

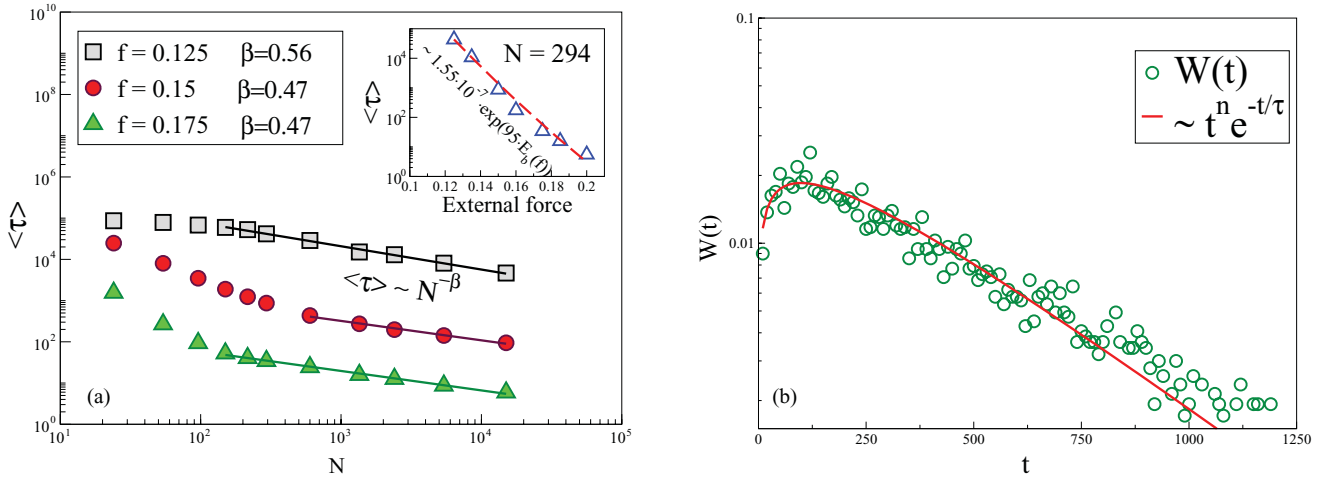

FIG. 7. (Color online) (a) Mean first breakage time $\langle\tau\rangle$ vs number of particles N in the membrane pulled with different tensile stress f as indicated. Symbols represent simulation data, whereas solid lines stand for fitting functions $\langle\tau\rangle \sim N^{-\beta}$. The inset shows force-dependent $\langle\tau\rangle$ for a membrane composed of $N = 294$ beads. (b) MFBT probability distribution $W(t)$ for the first scission of a bond in a flake with $N = 600$ particles at stress $f = 0.15$. Symbols denote the results of simulation, and the full line denotes for the fitting function $W(t) \propto t^n \exp(-t/\tau)$, with $n = 1/3$ and $\tau = 291.85$ t.u. Parameters of the heat bath are $T = 0.05$ and $\gamma = 0.25$.

brittle 2D sheet. We should like to point out that without self-healing, cf., Fig. 5(b), rupture time goes as $\langle\tau\rangle \propto N^{-\beta}$, with $\beta \approx 1$ (not plotted here), in contrast to the observed exponent $\beta \approx 0.5$.

It should be mentioned here that there is an interesting analogy between the observed power-law dependence of the MFBT time on system size and the power-law decrease of lifetime with system size in a thermally activated breakdown of fiber bundles [36,37]. In both our honeycomb network and in the fiber bundle model (FBM), the failure mechanism is related to a redistribution of load on neighboring bonds (fibers). Upon single rupture, bonds in our membrane are subject to a single scission threshold, whereas in the FBM there is a random distribution of tensile strengths. As a result, one finds a single value of $\beta \approx 0.5$ and an Arrhenian dependence of τ on temperature T in our elastic-brittle honeycomb network (see below), while the exponent β depends on the external load f and on T giving rise to a non-Arrhenian τ versus T relationship.

Note that the decline of MFBT τ in a topologically connected brittle system is by no means a trivial one. In a recent study [30] using MD simulation of a single anharmonic polymer chain subject to constant external tensile force, we found a rather complex interplay between the polymer chain dynamics and the resulting bond rupture probability distribution along the chain backbone. In a breakable chain (rather than a 2D network), it was observed that the corresponding power $\beta \to 0$ as $N \to \infty$. A major factor in this was attributed to nonlinear excitations as the possible origin for the observed increasing insensitivity of rupture time with respect to polymer length as the pulling force grows. One may thus conclude that nonlinear effects in bond scission are suppressed in 2D honeycomb networks.

One can also see from the inset in Fig. 7(a) that the MFBT τ decreases rapidly with growing stress f, that is, the energy barrier for rupture declines with f, in agreement with Eq. (5) and Zhurkov's experiments [35]. The probability distribution of MFBT $W(t)$ is shown in Fig. 7(b). It is well described by a Poisson probability distribution function $W(t) = 5.57 \times 10^{-3} t^{1/3} \exp(-t/291.85)$.

C. Cracks and mean failure time

The variation of τ_r, the mean failure time of the membrane with system size N, shown in Fig. 8(a) displays also a power-law dependence on system size N, $\langle\tau_r\rangle \propto N^{-\phi}$, whereby ϕ undergoes a crossover to a lower value beyond roughly $N > 300$. However, τ_r has a different physical meaning. Following Pomeau [38], the failure time can be approximately identified with the nucleation of a crack of critical size l_c given by Griffith's critical condition [24,39] assuming that crack propagation is much faster than the nucleation time. For a 2D geometry consisting of a flat brittle sheet with a crack perpendicular to the direction of stress, the potential energy per unit thickness of the sheet reads $U = -\frac{\pi l^2 f^2}{4Y} + 2\varepsilon l + U_0$, where Y is the Young modulus, ε is the surface energy needed to form a crack of length l, and U_0 is the elastic energy in the absence of stress ($f = 0$). This energy reaches a maximum for a critical crack length $l_c = \frac{4\varepsilon Y}{\pi f^2}$ beyond which no stable state exists except the separation of the sheet into two broken pieces. Thus, with a crack nucleation barrier $\Delta U = \frac{4\varepsilon^2 Y}{\pi f^2}$ (in 3D $\Delta U \propto f^{-4}$), the failure (ripoff) time $\tau_r = \tau_0 \exp(\Delta U_0/k_B T)$, as found in experiments with bidimensional microcrystals by Pauchard and Meunier [40] and in gels by Bonn *et al.* [41]. In Fig. 8(b), we present the variation of τ_r for membrane failure with stress f, in good agreement with the expected relationship $\Delta U \propto f^{-2}$. In addition, we show the variation of τ_r with temperature [see the inset in Fig. 8(b)], which is found to follow a well-expressed Arrhenian relationship with inverse temperature, in agreement with earlier studies [29,39].

As a rule, the end of the sheet rupturing process is marked by disintegration into two pieces of different size, so it is

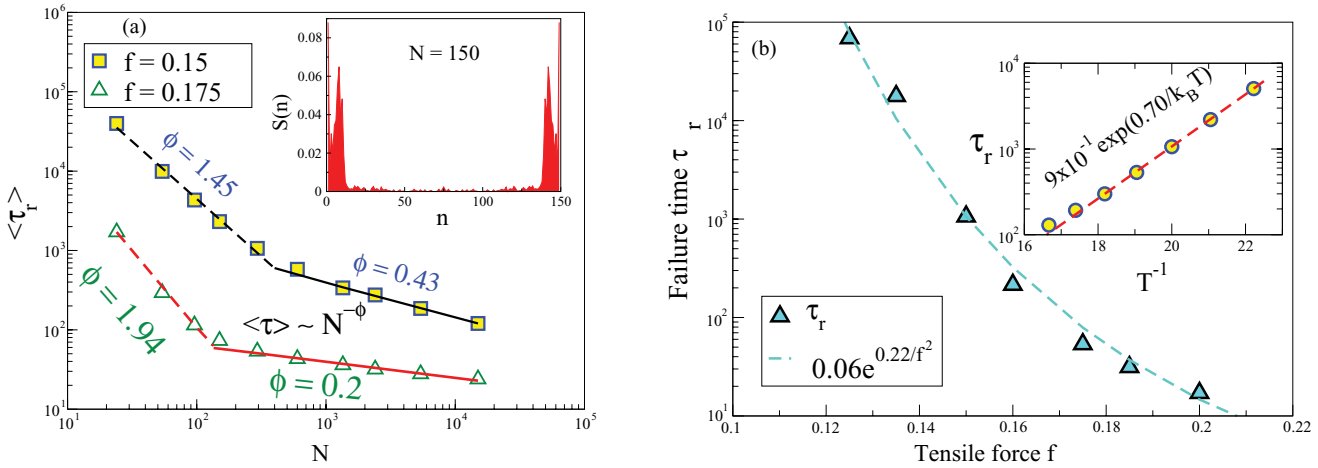

FIG. 8. (Color online) (a) Mean failure time $\langle \tau_r \rangle$ (time needed to split the membrane into two pieces) vs number of particles in the membrane for two values of the external pulling force f at $T = 0.05$ and $\gamma = 0.25$. Symbols denote simulation results and represent power-law fitting function $\langle \tau_r \rangle \sim N^{-\phi}$. The inset shows the PDF of the number of particles in the moment of splitting for a membrane composed of $N = 150$ beads. (b) Failure time $\langle \tau_r \rangle$ vs f in the case of $N = 294$. The inset shows variation of τ_r with inverse temperature (Arrhenian plot).

interesting to assess the size distribution of such fragments upon failure. In the inset in Fig. 8(a), we show a probability distribution $S(n)$ of the sizes of both fragments upon membrane ripoff. In a membrane composed of N beads, one observes a sharp bimodal distribution with narrow peaks at sizes $N_1 \approx 10$ and $N_2 \approx 140$. Evidently, for the adopted nearly radial direction—cf. Fig. 2(a)—of the applied tensile force, one always finds a pair of one small and another very large fragment.

One can readily verify from the typical topology of the observed cracks in the membrane, presented in Fig. 9, that (i) cracks usually emerge perpendicular to the direction of applied stress, and (ii) it is almost always the first row of nodes, to which the tensile force is immediately applied, that gets ripped off upon failure. Cracks that break the network sheet in the middle occur very seldom, in compliance with the sampled distribution of fragment sizes, $S(n)$ in the inset of Fig. 8(a). One would therefore predict a breakup of a protective cover spanned

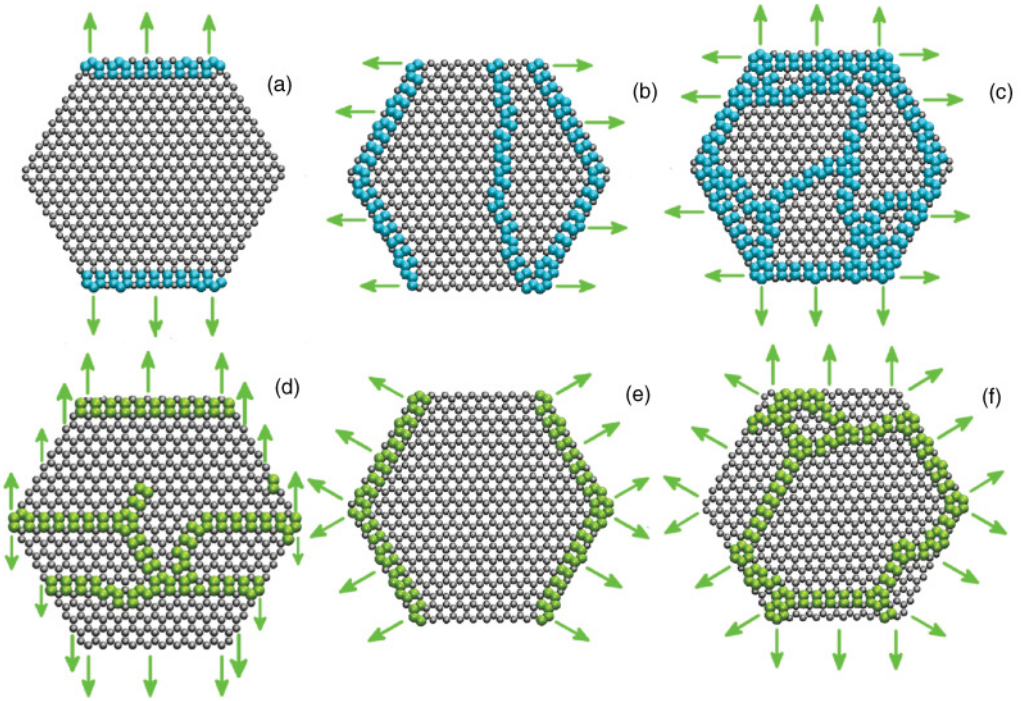

FIG. 9. (Color online) Overview of observed cracks in a honeycomb membrane composed of $N = 600$ particles for different orientation of the applied external pulling force. Green arrows indicate the orientation of the applied force ($f = 0.15$): (a),(b),(d) uniaxial; (c) biaxial; (e),(f) slanted. Parameters of a heat bath are $T = 0.05$ and $\gamma = 0.25$. The typical cracks are marked in color on the geometrically undistorted arrangement of network nodes for better visibility.

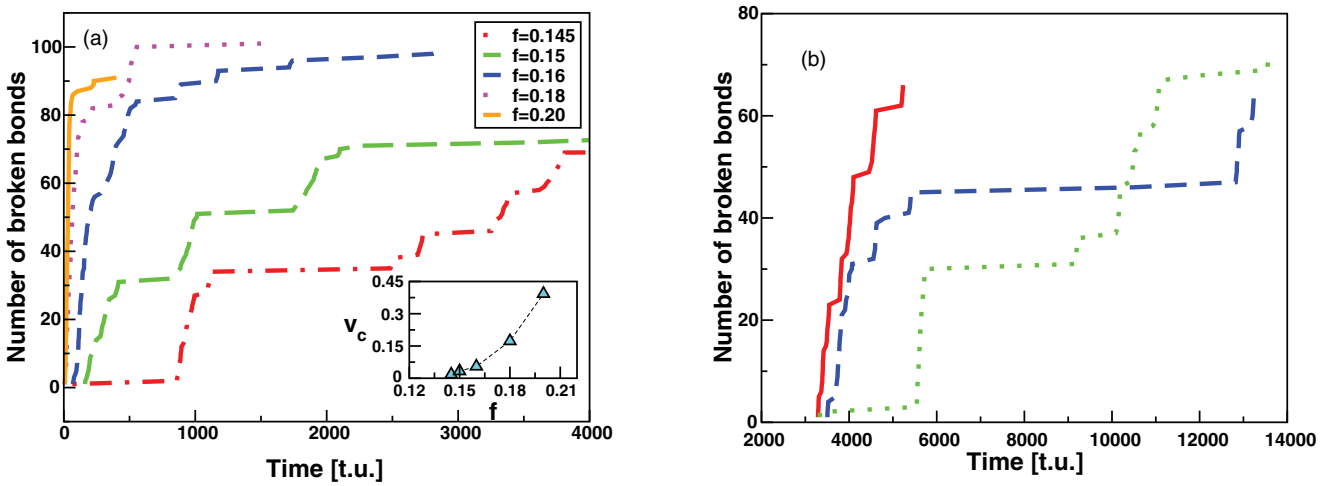

FIG. 10. (Color online) (a) Crack propagation velocity (number of broken bonds per unit time) for a membrane with $N = 600$ beads at different strength of the external force f as indicated. (b) Three different realizations of cracks at applied force $f = 0.14$. The inset shows a variation of the mean crack propagation velocity with f. Here $T = 0.05$ and $\gamma = 0.25$.

on the orifice of a tube like the one shown in Fig. 9 to proceed immediately at the fixed orbicular boundary where the tensile force applies to the network. It is interesting to note that the geometry of cracks in the membrane shown in Fig. 9 appears very similar to that observed in drying-induced cracking of thin layers of materials subject to structural disorder [42].

The emerging cracks are expected to propagate with a speed that increases as the strength of the external force is increased, as the inset in Fig. 10(a) indicates. In fact, in Fig. 10(a) one observes typical curves comprising a series of short intervals with steep growth of the number of broken bonds per unit time and longer horizontal "terraces" preceding the nucleation of a new crack. Even though the data, presented in Fig. 10(a), are not averaged over many realizations, and, as Fig. 10(b) suggests, individual realizations of propagating cracks may strongly differ even at the same stress f, a general increase of the propagation velocity with growing external force f (see the inset) can be unambiguously detected, in agreement with earlier observations [20].

For our model membrane with computed Young modulus $Y \approx 0.02$, we get for the Rayleigh wave speed $c_R \approx 0.14$. Thus for most of the applied tensile stress values, we observe crack propagation at a speed less than c_R [inset in Fig. 10(b)]. As argued by Ref. [43], propagation speed cannot exceed c_R because the crack splits off into multiple cracks before reaching c_R. In contrast, Abraham and Gao in Ref. [44] have reported on cracks that can travel faster than the Rayleigh speed. Thus, our rough estimates (inset in Fig. 10) agree well with data from the literature. Converting our results to proper metric units, with bond length $\sigma \approx 0.144$ nm and energy $\approx 20 k_B T$, which yields 1 MD t.u. $\approx 10^{-12}$ s, we estimate the typical crack propagation speed to be $v_c \approx 50$ m/s. Note that the mean crack speed for natural latex rubber was given as 56 m/s [45].

IV. SUMMARY

In the present work, we have studied the bond rupture and ensuing fracture of a honeycomb brittle membrane subject to uniform radially applied external stretching forces for different values of force f, temperature T, and membrane size N. The most important conclusions that can be drawn from our molecular-dynamics simulation can be summarized as follows:

(i) Bonds scission in hexagonal 2D sheets with a honeycomb structure of the underlying network subjected to external pulling perpendicular to the flake's edges takes place overwhelmingly at the sheet periphery.

(ii) The mean first breakage time of breaking bonds depends on membrane size N as a power law, $\tau \propto N^{-\beta}$, with $\beta \approx 0.50 \pm 0.03$.

(iii) The failure time τ_r until a brittle sheet disintegrates into pieces follows a power law too, $\tau \propto N^{-\phi(f)}$, and an exponential decay $\tau_r \propto \exp(\text{const}/f^2)$ upon increasing strength of the pulling force, in agreement with Griffith's criterion for failure.

(iv) Cracks emerge in the vicinity of the membrane edges and typically propagate parallel to the edges, splitting the sheet in two pieces with a size ratio of $\approx 7\%$.

(v) Crack propagation speed is observed to increase rapidly with tensile force.

We believe that these findings can be seen as generic also for 2D network brittle sheets of different geometry (hexagonal lattices, or quadratic lattices with second-nearest-neighbor bonding) where a similar interplay between elastic and fracture behavior is expected to take place. It is clear, however, that more investigations are needed before a full understanding of fracture in such systems is achieved.

ACKNOWLEDGMENTS

The authors would like to thank V. G. Rostiashvili for fruitful discussions. A.M. gratefully acknowledges support by the Max Planck Institute for Polymer Research during the time of this investigation. This study has been supported by the Deutsche Forschungsgemeinschaft (DFG), Grants No. SFB625/B4 and No. FOR597. H.P. and A.M. acknowledge the use of computing facilities of Madara Computer Center at Bulg. Acad. Sci.

[1] R. P. Sijbesma, F. H. Beijer, L. Brunsveld, B. J. B. Folmer, J. H. K. K. Hirschberg, R. F. Lange, J. K. L. Lowe, and E. W. Meijer, Science **278**, 1601 (1997).

[2] R. P. Sijbesma and E. W. Meijer, Chem. Commun. **1**, 5 (2003).

[3] M. Neek-Amal and F. M. Peeters, Phys. Rev. B **81**, 235437 (2010); **82**, 085432 (2010); Appl. Phys. Lett. **97**, 153118 (2010).

[4] H. Zhao, K. Min, and N. R. Aluru, Nano Lett. **9**, 3012 (2009); H. Zhao and N. R. Aluru, J. Appl. Phys. **108**, 064321 (2010); K. Min and N. R. Aluru, Appl. Phys. Lett. **98**, 013113 (2011).

[5] S. Chen, L. Brown, M. Levendorf, W. Cai, S.-Y. Ju, J. Edgeworth, X. Li, C. W. Magnuson, A. Velamakanni, R. D. Piner, J. Kang, J. Park, and R. S. Ruoff, ACS Nano **5**, 1321 (2011).

[6] M. Pumera, Mater. Today **14**, 308 (2011).

[7] D.-E. Jiang, V. R. Cooper, and S. Dai, Nano Lett. **9**, 4019 (2009).

[8] A. S. Barnard and I. K. Snook, J. Chem. Phys. **128**, 094707 (2008).

[9] J. C. Hansen, R. Skalak, S. Chien, and A. Hoger, Biophys. J. **70**, 146 (1996).

[10] P. D. Beale and D. J. Srolovitz, Phys. Rev. E **37**, 5500 (1988).

[11] M. J. Saxton, Biophys. J. **57**, 1167 (1990).

[12] D. H. Boal, U. Seifert, and A. Zilker, Phys. Rev. Lett. **69**, 3405 (1992).

[13] P. Meakin, G. Li, L. M. Sander, E. Luis, and F. Guinea, J. Phys. A **22**, 1393 (1989).

[14] L. Monette and M. P. Anderson, Modell. Simul. Mater. Sci. **2**, 53 (1994).

[15] M. Dao, J. Li, and S. Suresh, Mater. Sci. Eng., C **26**, 1232 (2006).

[16] D. S. Argyropoulos and H. I. Bolker, Macromolecules **20**, 2915 (1987); Macromol. Chem. **189**, 607 (1988).

[17] L. Barral, F. J. Diez, S. Garcia-Garabal, J. Lopez, B. Montero, R. Montes, C. Ramirez, and M. Rico, Europ. Polym. J. **41**, 1662 (2005).

[18] Z. Zhang, G. Liang, P. Ren, and J. Wang, Polymer Compos. **28**, 755 (2007).

[19] K. Chenoweth, S. Cheung, A. C. T. van Duin, W. A. Goddard III, and E. M. Kober, J. Am. Chem. Soc. **127**, 7192 (2005).

[20] D. Holland and M. Marder, Phys. Rev. Lett. **80**, 746 (1998).

[21] A. Mattoni, L. Colombo, and F. Cleri, Phys. Rev. Lett. **95**, 115501 (2005).

[22] M. J. Buehler, H. Tang, A. C. T. van Duin, and W. A. Goddard III, Phys. Rev. Lett. **99**, 165502 (2007).

[23] M. J. Alava, P. K. Nukala, and S. Zapperi, Adv. Phys. **55**, 349 (2006).

[24] A. A. Griffith, Philos. R. Soc. London A **221**, 163 (1920).

[25] S. Santucci, L. Vanel, A. Guarino, R. Scorretti, and S. Ciliberto, Europhys. Lett. **62**, 320 (2003).

[26] Z.-G. Wang, U. Landman, R. L. Blumberg Selinger, and W. M. Gelbart, Phys. Rev. B **44**, 378 (1991).

[27] R. L. Blumberg Selinger, Z.-G. Wang, W. M. Gelbart, and A. Ben-Shaul, Phys. Rev. A **43**, 4396 (1991).

[28] G. Gagnon, J. Patton, and D. J. Lacks, Phys. Rev. E **64**, 051508 (2001).

[29] C. L. Dias, J. Kröger, D. Vernon, and M. Grant, Phys. Rev. E **80**, 066109 (2009).

[30] J. Paturej, A. Milchev, V. G. Rostiashvili, and T. A. Vilgis, Europhys. Lett. **94**, 48003 (2011).

[31] J. Paturej, A. Milchev, V. G. Rostiashvili, and T. A. Vilgis, J. Chem. Phys. **134**, 224901 (2011).

[32] A. Milchev, J. Paturej, V. G. Rostiashvili, and T. A. Vilgis, Macromolecules **44**, 3981 (2011).

[33] A. Ghosh, D. I. Dimitrov, V. G. Rostiashvili, A. Milchev, and T. A. Vilgis, J. Chem. Phys. **132**, 204902 (2010).

[34] S. S. Brenner, J. Appl. Phys. **33**, 33 (1962).

[35] S. N. Zhurkov, Int. J. Fracture Mech. **1**, 311 (1965).

[36] N. Yoshioka, F. Kun, and N. Ito, Phys. Rev. Lett. **101**, 145502 (2008).

[37] N. Yoshioka, F. Kun, and N. Ito, Phys. Rev. E **82**, 055102(R) (2010).

[38] Y. Pomeau, C. R. Acad. Sci. Paris II **314**, 553 (1992).

[39] A. Rabinovich, M. Friedman, and D. Bahat, Europhys. Lett. **67**, 969 (2004).

[40] L. Pauchard and J. Meunier, Phys. Rev. Lett. **70**, 3565 (1993).

[41] D. Bonn, H. Kellay, M. Prochnow, K. Ben-Djemiaa, and J. Meunier, Science **280**, 265 (1998).

[42] G. Villalobos, F. Kun, and J. D. Munoz, Phys. Rev. E **84**, 041114 (2011).

[43] J. Fineberg, S. P. Gross, M. Marder, and H. L. Swinney, Phys. Rev. Lett. **67**, 457 (1991).

[44] F. F. Abraham and H. Gao, Phys. Rev. Lett. **84**, 3113 (2000).

[45] P. J. Petersan, R. D. Deegan, M. Marder, and H. L. Swinney, Phys. Rev. Lett. **93**, 015504 (2004).